

Extension of the Non-Crossing Approximation for the Anderson Model with Finite Coulomb Repulsion

Junya OTSUKI* and Yoshio KURAMOTO

Department of Physics, Tohoku University, Sendai 980-8578

(Received March 23, 2022)

The non-crossing approximation (NCA) is generalized for the Anderson model with finite Coulomb repulsion U . Resummation of infinite number of terms is performed so as to incorporate all leading contributions in the limit of large degeneracy of the local states. With negligible weight of the doubly occupied local states in equilibrium, the extension is achieved through simple modifications of the lowest order formulae. The single-particle excitation spectrum is calculated with almost the same computational effort as in the original NCA. The present scheme reproduces the scaling behavior of the Kondo resonance in the density of states, and gives reasonable description of thermodynamics of the finite- U Anderson model over a wide range of temperature.

KEYWORDS: non-crossing approximation (NCA), Anderson model, single-particle excitation spectrum, entropy, specific heat, resolvent method

1. Introduction

Heavy fermion systems, where $4f$ electrons play an important role, show plenty of fascinating phenomena. Such systems are often modeled by the periodic Anderson model, which exhibits the Kondo effect as well as the mixed-valence property. The single-impurity Anderson model is utilized in the intermediate stage for solving the periodic model by means of the dynamical mean field theory (DMFT).¹ Combined with band calculations, the DMFT can give a semi-quantitative description of density of states in real compounds.^{2–4} For this purpose, it is required to solve the impurity model under realistic conditions for system parameters, which may lead to a heavy load in numerical calculation. Hence it is still important to develop a simple but reliable computational scheme to solve the impurity Anderson model, although low-energy properties of the model have now been understood well.

Perturbation theory with respect to the hybridization can take into account strong correlations between local electrons.^{5–9} The lowest order self-consistent approximation is called the non-crossing approximation (NCA), since the scheme incorporates all diagrams without crossing of conduction lines. In the case of large degeneracy n of the local states, the NCA derives proper dynamics as well as thermodynamics of the Anderson model with infinite Coulomb repulsion U . The NCA accordingly plays a role complementary to the numerical renormalization group (NRG)¹⁰ and the quantum Monte Carlo (QMC),¹¹ since the latter numerical methods are only available in the small n case by restriction of computational time. Combination of the NCA and the DMFT has so far revealed various characteristics of the periodic Anderson model^{12,13} and the Hubbard model.¹⁴

The NCA is originally derived for the infinite- U Anderson model, where only $4f^0$ and $4f^1$ states are contained. For practical use, however, additional informations on $4f^2$ states are necessary as well. Extension of the NCA

to the finite- U case has been tried in several ways.^{15–18} It has been found that increase of the Kondo temperature, which should occur due to the involvement of $4f^2$ states, cannot be reproduced by lower order modification of the NCA to the finite- U case, even though n is large.¹⁵ Therefore, higher order terms are relevant in such models.

Sakai *et al.* have pointed out importance of infinite number of skeleton diagrams in large- n limit, and has called their approximation NCA f^2v .¹⁵ The theory seems to yield a proper energy scale of the Kondo effect. However, the resummation procedure for the single-particle excitation spectrum does not give a conserving approximation. Haule *et al.* have developed a conserving approximation by selecting a set of generating functionals.¹⁸ It is called symmetrized finite- U NCA (SUNCA), since the approximation incorporates excitations of both particles and holes on equal footing, and can accordingly reproduce the symmetric feature of the single-particle excitation spectrum. Although the theory provides a proper energy scale in $n = 2$, actual computation is not easy for large n even for a simple structure of the conduction band.

In order to be applied to realistic impurity models with complex $4f$ -shell and band structures, or to the DMFT as a solver of the single-impurity problem, the practical calculational scheme should be simple enough. In this paper, we modify the NCA f^2v scheme so as to recover the conserving property in the limit of large n , and present results for the single-particle spectra. The computations require almost the same effort as in the original NCA. It will be shown that the theory gives a proper energy scale and characteristics of the Kondo effect under the large- n condition. In addition we check the accuracy of the theory in thermodynamics.

This paper is organized as follows. Section 2 introduces a model that we will consider in this paper, and gives a brief description of the resolvent method. Formulations for the single-particle excitation are given in §3. In §4,

*E-mail address: otsuki@cmpt.phys.tohoku.ac.jp

we present numerical results, and discuss their accuracy in several aspects. In the final section, we summarize characteristics of the present theory.

2. Model and Resolvent Method

We consider the Anderson model with an orbital degeneracy in the local states, which are called $4f$ states hereafter. Assuming strong Hund's coupling, we distinguish the $4f$ states by a single quantum number α with n -fold degeneracy, e.g., the azimuthal component of the total angular momentum $j = 5/2$. Conduction electrons hybridize with $4f$ electrons having the same index α . Then, the Hamiltonian takes the form

$$H = \sum_{\mathbf{k}\alpha} \epsilon_{\mathbf{k}} c_{\mathbf{k}\alpha}^\dagger c_{\mathbf{k}\alpha} + \epsilon_f \sum_{\alpha} f_{\alpha}^\dagger f_{\alpha} + \frac{U}{2} \sum_{\alpha \neq \alpha'} f_{\alpha}^\dagger f_{\alpha} f_{\alpha'}^\dagger f_{\alpha'} + \sum_{\mathbf{k}\alpha} V_{\mathbf{k}} f_{\alpha}^\dagger c_{\mathbf{k}\alpha} + \text{h.c.}, \quad (1)$$

where $c_{\mathbf{k}\alpha}$ and f_{α} is annihilation operators for the conduction electron and the $4f$ electron, respectively.

We work under the large- U condition, and accordingly restrict $4f$ states to $4f^0$, $4f^1$ and $4f^2$. In order to take account of the strong correlation between $4f$ electrons, we introduce the resolvent $R_{\gamma}(z)$ for each $4f$ state as follows:

$$R_{\gamma}(z) = [z - \epsilon_{\gamma} - \Sigma_{\gamma}(z)]^{-1}, \quad (2)$$

where γ indicates either $4f^0$, $4f^1$ or $4f^2$ states, and hereafter we use corresponding indices 0, 1 or 2, respectively. ϵ_{γ} is the unperturbed energy, i.e., $\epsilon_0 = 0$, $\epsilon_1 = \epsilon_f$ and $\epsilon_2 = 2\epsilon_f + U$. The hybridization is to be included in the self-energy part $\Sigma_{\gamma}(z)$ by the self-consistent perturbation theory.⁵⁻⁸

Once the resolvent is obtained, physical quantities are computed with use of them.⁵⁻⁸ For example, the partition function Z_f of $4f$ part is given by

$$Z_f = \int_C \frac{dz}{2\pi i} e^{-\beta z} \sum_{\gamma} R_{\gamma}(z), \quad (3)$$

where the contour C encircles all the singularities of $R_{\gamma}(z)$ counter-clockwise. The resolvent is utilized to calculate dynamics as well.

Throughout this paper, we give formulations on the assumption that there is no splitting in $4f^1$ or $4f^2$ levels for simplicity. Alternative formulations with such splittings are obtained straightforwardly by distinguishing resolvents for each split level.

3. Finite- U Perturbation Theory

The excitations of the conduction holes always accompany a summation of $4f^1$ or $4f^2$ states, which produces a factor n or $n-1$, respectively. Hence from viewpoint of the $1/n$ expansion, the hole excitations are not in higher order in perturbation series, and proper account should be taken of consecutive occurrences of such excitations. Since $4f^0$ - $4f^1$ fluctuation terms are represented by the diagrams without crossing of conduction lines, they are counted by the self-consistent treatment of the lowest order skeleton diagrams. On the other hand, $4f^1$ - $4f^2$ fluctuations involve crossing of conduction lines. Conse-

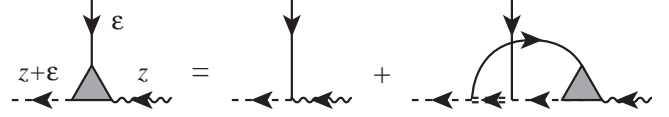


Fig. 1. Diagrammatic representation of the equation for the vertex function. Solid, wavy, dashed and double dashed line represent conduction electron, $4f^0$, $4f^1$ and $4f^2$ resolvent, respectively. All resolvents are regarded as renormalized ones.

quently, higher order skeleton diagrams are necessary to take account of such terms.

In this section, we present an extended theory where $4f^1$ - $4f^2$ fluctuations accompanying conduction holes are included properly. We first review the theory by Sakai *et al.* where a vertex part is introduced for the self-energy. After a brief description is given of a relation to the theory by Haule *et al.*, we proceed to the formulation of the single-particle excitation.

3.1 The NCA f^2v scheme

Before we present formulations for the single-particle excitation, we summarize the NCA f^2v scheme developed by Sakai *et al.*^{4,15} In order to derive the self-energy, they have introduced the vertex part $\Lambda(z, \epsilon)$ which consists of the $4f^1$ - $4f^2$ fluctuations with consecutive excitations of conduction holes:

$$\Lambda(z, \epsilon) = 1 + (n-1) \int d\epsilon' W(\epsilon') f(\epsilon') R_1(z + \epsilon') \times R_2(z + \epsilon + \epsilon') \Lambda(z, \epsilon'), \quad (4)$$

where $f(\epsilon)$ is the Fermi distribution function and $W(\epsilon)$ is defined by $W(\epsilon) = \sum_{\mathbf{k}} |V_{\mathbf{k}}|^2 \delta(\epsilon - \epsilon_{\mathbf{k}})$. Equation (4) is diagrammatically represented by Fig. 1. The vertex part can equally be represented by diagrams with all arrows reversed in Fig. 1.

A computation of the function $\Lambda(z, \epsilon)$ with double argument takes a lot of time. Sakai *et al.* have pointed out that the energy dependence of $R_2(z)$ is less important than $R_1(z)$'s in eq. (4), and proposed an approximation where $R_2(z)$ is replaced by a constant value $\tilde{R}_2 = R_2^{(0)}(\epsilon_f)$, which is the bare resolvent of $4f^2$ state at $z = \epsilon_f$. In this approximation, the vertex part is independent of the energy of conduction electrons, and becomes a function of single argument written as $\Lambda(z)$. Equation (4) is then solvable and leads to an expression

$$\Lambda(z) = [1 - (n-1) \tilde{R}_2 \tilde{\Sigma}_0^{(\text{NCA})}(z)]^{-1}, \quad (5)$$

where $\tilde{\Sigma}_0^{(\text{NCA})}(z)$ is defined by

$$\tilde{\Sigma}_0^{(\text{NCA})}(z) = \int d\epsilon W(\epsilon) f(\epsilon) R_1(z + \epsilon), \quad (6)$$

which is the self-energy of $4f^0$ state in the NCA divided by n . The approximated vertex function $\Lambda(z)$ is now analytic in the region except for $\text{Im}z = 0$, while original one $\Lambda(z, \epsilon)$ has the additional cut at $\text{Im}(z + \epsilon) = 0$ coming from $R_2(z)$.

The self-energy part of each state is represented with use of the vertex part introduced above. The self-energy of $4f^0$ state is obtained by multiplying the NCA self-

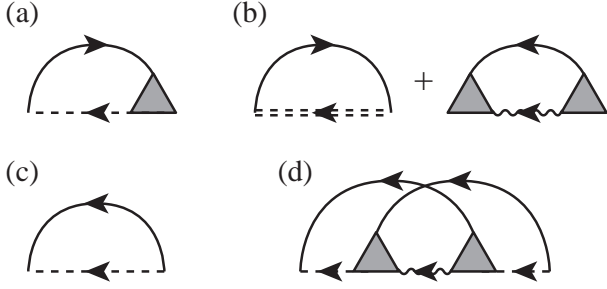


Fig. 2. Diagrammatic representation of the self-energy (a) $\Sigma_0(z)$, (b) $\Sigma_1(z)$, (c) $\Sigma_2(z)$, and (d) a correction term which should be included in $\Sigma_2(z)$ for construction of a conserving approximation.

energy and the vertex function $\Lambda(z)$ as follows:

$$\Sigma_0(z) = n\tilde{\Sigma}_0^{(\text{NCA})}(z)\Lambda(z). \quad (7)$$

Corresponding diagrammatic representation is given by Fig. 2(a). Figure 2(b) shows a diagram of $4f^1$ self-energy, whose analytic expression is

$$\begin{aligned} \Sigma_1(z) = & \int d\epsilon W(\epsilon)[1 - f(\epsilon)]\tilde{R}_0(z - \epsilon) \\ & + (n - 1) \int d\epsilon W(\epsilon)f(\epsilon)R_2(z + \epsilon), \end{aligned} \quad (8)$$

where $\tilde{R}_0(z)$ is defined by

$$\tilde{R}_0(z) = R_0(z)\Lambda(z)^2. \quad (9)$$

Introduction of the auxiliary function $\tilde{R}_0(z)$ makes eq. (8) look similar to the lowest order self-energy. The self-energy of $4f^2$ states are evaluated without any vertex corrections by

$$\Sigma_2(z) = 2 \int d\epsilon W(\epsilon)[1 - f(\epsilon)]R_1(z - \epsilon), \quad (10)$$

which is expressed by the diagram of Fig. 2(c). The term shown in Fig. 2(d) is actually required for a construction of the conserving approximation as we will discuss later. We neglect the term, however, since its contribution is of order $1/n^2$ at most. Thus we avoid the double integral with respect to the energy of conduction electrons that would take much time. The self-energy in the $\text{NCA}f^2v$ consequently contains all diagrams of the leading contributions in the large- n limit, while the original NCA for the infinite- U model incorporates diagrams up to the first order of $1/n$.

Resultant $\text{NCA}f^2v$ equations have forms quite similar to that of the simplest finite- U extension in spite of the resummation of all the leading contributions. The only modification of the equations is the replacement of $\Sigma_0(z)$ and $R_0(z)$ by $\Sigma_0(z)\Lambda(z)$ and $R_0(z)\Lambda(z)^2$, respectively. The vertex function $\Lambda(z)$ has been given analytically by eq. (5). Accordingly, the computational effort is almost the same as in the lowest order self-consistent approximation without vertex corrections.

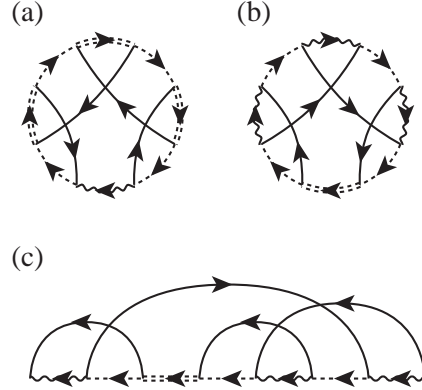


Fig. 3. Eighth order diagrams of the generating functionals (a) considered in both the SUNCA and the $\text{NCA}f^2v$, and (b) considered in the SUNCA but not in the $\text{NCA}f^2v$. Diagram (c) represents one of contributions to the $4f^1$ state self-energy derived from the functional (b), which is of order $1/n^3$.

3.2 Relation to the SUNCA

Haule and coworkers have extended the NCA to the finite- U case, and called the scheme SUNCA.¹⁸ They have constructed a conserving scheme by taking a set of infinite number of generating functionals into consideration. We discuss relation between the SUNCA and the $\text{NCA}f^2v$.

The generating functionals in the SUNCA consist of two parts except for terms less than the sixth order. Figures 3(a) and (b) show diagrams of the eighth order generating functionals that the SUNCA incorporates. The functional (a) generates the self-energy terms included in the $\text{NCA}f^2v$. On the other hand, the $\text{NCA}f^2v$ does not incorporate contributions generated from the functional (b). Figure 3(c) shows one of the eighth order terms of the $4f^1$ state self-energy derived from the functional (b). It includes three conduction electrons propagating forward, and accordingly is of order $1/n^3$. Corresponding vertex part coming from the (b)-type generating functionals consists of the $4f^0$ - $4f^1$ fluctuations with consecutive excitations of forward propagating conduction electrons. Hence perturbation series of the self-energy generated from the (b)-type functionals are of order $1/n$ at most. Consequently, large- n condition justifies the neglect of (b)-type diagrams, which are relevant in the small- n case, especially $n = 2$.

It is noticed that the $\text{NCA}f^2v$ itself is a conserving scheme provided no further approximation is made such as simplification of the vertex part and neglect of the correction term for $\Sigma_2(z)$. Since these approximations are justified under the condition of large- n and large- U , we expect that violation of the conserving property is not serious under such condition.

3.3 Single-particle Green function

We now proceed to the single-particle excitation. The $4f$ electron Green function is represented in terms of the X -operator $X_{\gamma\gamma'} = |\gamma\rangle\langle\gamma'|$ as follows:

$$G_f(\tau) = - \sum_{\gamma\gamma'\gamma''\gamma'''} \langle\gamma|f_\alpha|\gamma'\rangle\langle\gamma''|f_\alpha^\dagger|\gamma'''\rangle$$

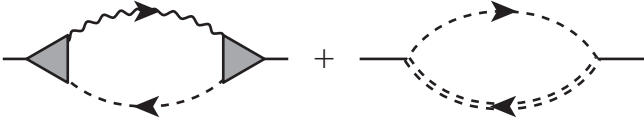


Fig. 4. Diagrammatic representation of the 4f electron Green function.

$$\times \langle T_\tau X_{\gamma\gamma'}(\tau) X_{\gamma''\gamma'''} \rangle, \quad (11)$$

where $X_{\gamma\gamma'}(\tau)$ is in the Heisenberg picture. The Green function is now independent of quantum number α . After the Fourier transformation, the Green function $G_f(i\epsilon_n)$ is to be derived with use of the resolvents,⁵⁻⁸ where $\epsilon_n = (2n+1)\pi T$ is the Matsubara frequency.

In order to construct a consistent approximation, infinite terms should be considered in the single-particle Green function as in the self-energy. The original NCA f^2v scheme, however, does not take proper account of the vertex correction. An appropriate formula of the Green function is given by

$$G_f(i\epsilon_n) = \frac{1}{Z_f} \int_C \frac{dz}{2\pi i} e^{-\beta z} \tilde{R}_0(z) R_1(z + i\epsilon_n) + (n-1) \frac{1}{Z_f} \int_C \frac{dz}{2\pi i} e^{-\beta z} R_1(z) R_2(z + i\epsilon_n), \quad (12)$$

where the contour C encircles $\text{Im}z = 0$ and $\text{Im}z = -i\epsilon_n$ counter-clockwise, and $\tilde{R}_0(z)$ is defined by eq. (9). Since the vertex function $\Lambda(z)$ is independent of the energy of the conduction electron and has the same analyticity as $R_0(z)$ in the present approximation, the Green function has been given simply by replacing $R_0(z)$ with $\tilde{R}_0(z)$ in the lowest order formula. Corresponding diagram is represented by Fig. 4. We note that the first term of right-hand side of eq. (12) contains not only diagonal components $\langle T_\tau X_{01}(\tau) X_{10} \rangle$ and $\langle T_\tau X_{12}(\tau) X_{21} \rangle$, but also off-diagonal components $\langle T_\tau X_{12}(\tau) X_{10} \rangle$ and $\langle T_\tau X_{01}(\tau) X_{21} \rangle$ when the vertex part is expanded.

Performing the integral with respect to z and analytic continuation $i\epsilon_n \rightarrow \omega + i\delta$ onto real frequencies in eq. (12), we obtain the single-particle excitation spectrum $\rho_f(\omega) = -\pi^{-1} \text{Im} G_f(\omega + i\delta)$ as follows:

$$\rho_f(\omega) = \int d\epsilon [\tilde{\xi}_0(\epsilon) \eta_1(\epsilon + \omega) + \tilde{\eta}_0(\epsilon) \xi_1(\epsilon + \omega)] + (n-1) \int d\epsilon [\xi_1(\epsilon) \eta_2(\epsilon + \omega) + \eta_1(\epsilon) \xi_2(\epsilon + \omega)]. \quad (13)$$

We have included spectral functions of the resolvent $\eta_\gamma(\omega)$ and those of the defect propagator $\xi_\gamma(\omega)$ defined by

$$\eta_\gamma(\omega) = -\pi^{-1} \text{Im} R_\gamma(\omega + i\delta), \quad (14)$$

$$\xi_\gamma(\omega) = Z_f^{-1} e^{-\beta\omega} \eta_\gamma(\omega + i\delta). \quad (15)$$

Analogously, $\tilde{\eta}_0(\omega)$ and $\tilde{\xi}_0(\omega)$ are defined from $\tilde{R}_0(z)$. Since it is awkward to compute $\xi_\gamma(\omega)$ by eq. (15) due to the Boltzmann factor, $\xi_\gamma(\omega)$ should be calculated by another set of equations which are obtained by transforming the original ones (see Appendix).

3.4 Sum-rules

The single-particle spectrum obtained within conserving scheme satisfies the following exact sum-rules:

$$\int d\omega f(\omega) \rho_f(\omega) = \langle X_{11} \rangle + (n-1) \langle X_{22} \rangle = \frac{n_f}{n}, \quad (16)$$

$$\int d\omega [1 - f(\omega)] \rho_f(\omega) = \langle X_{00} \rangle + (n-1) \langle X_{11} \rangle, \quad (17)$$

where n_f is the average number of 4f electrons. $\langle X_{\gamma\gamma} \rangle$ is an average occupation of γ state, and is given in terms of $\xi_\gamma(\omega)$ by

$$\langle X_{\gamma\gamma} \rangle = \int d\omega \xi_\gamma(\omega). \quad (18)$$

The sum-rule of eq. (16) follows from the fact that the left-hand side corresponds to $G_f(-0)$ in eq. (11). Similarly the left-hand side of eq. (17) corresponds to $G_f(+0)$. Equation (16) has an intuitive interpretation that the 4f¹ states are occupied in proportion to $n \langle X_{11} \rangle$, and the 4f² states in proportion to $n(n-1) \langle X_{22} \rangle / 2$. Equations (16) and (17) lead to another sum-rule of the form

$$\int d\omega \rho_f(\omega) = \langle X_{00} \rangle + n \langle X_{11} \rangle + (n-1) \langle X_{22} \rangle. \quad (19)$$

The sum-rule for $\xi_\gamma(\omega)$, given by eq. (A-8), ensures that the integral of $\rho_f(\omega)$ is always less than unity. It is clear that the lowest order formula of the Green function satisfies the sum-rule, eqs. (16), (17) and (19), as in the original NCA.⁵ The fact may imply that any correction terms in the Green function should not affect the integrated spectral intensity.

We now discuss whether the density of states given by eq. (13) satisfies the exact sum-rule in the present theory. We can see from eqs. (5) and (9) that $\tilde{R}_0(z)$ behaves at infinity as $\lim_{|z| \rightarrow \infty} \tilde{R}_0(z) = z^{-1}$, similarly to $R_\gamma(z)$. The asymptotic behavior leads to the following sum-rule for $\tilde{R}_0(z)$:

$$\int d\omega \tilde{\eta}_0(\omega) = 1. \quad (20)$$

Equation (20) ensures that the particle number is not affected by the vertex correction, and is given by eq. (16). On the other hand, the approximate vertex correction changes the total intensity. Equation (17) is modified due to the vertex correction by

$$\int d\omega [1 - f(\omega)] \rho_f(\omega) = \langle \tilde{X}_{00} \rangle + (n-1) \langle X_{11} \rangle, \quad (21)$$

where $\langle \tilde{X}_{00} \rangle$ is defined with use of $\tilde{\xi}_0(\epsilon)$ in a manner similar to eq. (18). Equation (21) follows from eq. (13). If $\langle \tilde{X}_{00} \rangle$ were the same as $\langle X_{00} \rangle$, the exact sum-rule in eqs. (16), (17) and (19) would be satisfied. The spectral intensity in our framework is examined by numerical calculation in the next section.

4. Numerical Results and Discussions

In this section, we present numerical results for single-particle excitation spectrum and thermodynamic quantities. Then we shall examine accuracy of the present theory. We take a rectangular model $W(\epsilon) = W_0 \theta(D - |\epsilon|)$ with half width of conduction band being D . The degen-

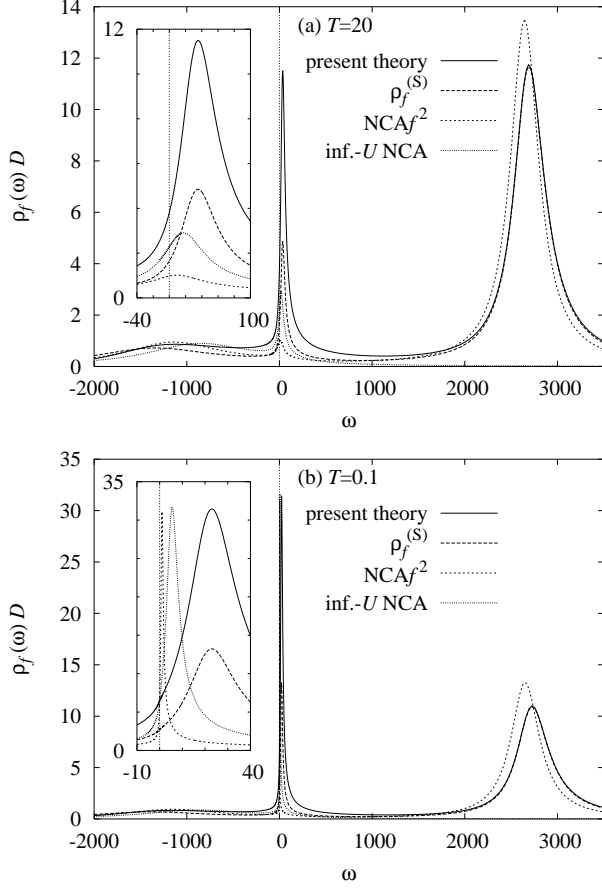


Fig. 5. Single-particle spectra computed in the several schemes with parameters $n = 6$, $W_0 = 30$, $\epsilon_f = -1200$ and $U = 3|\epsilon_f| = 3600$ at temperatures (a) $T = 20$ and (b) $T = 0.1$.

eracy n takes $n = 6$ and $n = 4$. We take a unit such that $D = 10^4$ throughout this paper. One may imagine the energy unit as of the order of Kelvin to meV for correspondence with actual systems. Parameters W_0 , ϵ_f and U are varied in the range where the $4f$ particle number is almost unity.

4.1 Single-particle excitation spectrum

We first show numerical results for density of states $\rho_f(\omega)$ of $4f$ electrons. In addition to results in the present scheme, results in the other schemes are shown for comparison: (i) $\rho_f^{(S)}$, which considers the vertex correction in the self-energy of resolvents but not in the Green function,^{4,15} (ii) $\text{NCA}f^2$, which is the lowest order self-consistent approximation including $4f^2$ states but without the vertex correction, and (iii) infinite- U NCA, which is the original NCA with infinite Coulomb repulsion.

Figure 5 shows single-particle excitation with parameters $n = 6$, $W_0 = 30$, $\epsilon_f = -1200$ and $U = 3|\epsilon_f| = 3600$ at temperatures $T = 20$ and $T = 0.1$. In the $\text{NCA}f^2$, the peak of $4f^2$ states is slightly sharper and is located at lower energy than the other schemes. There is no significant difference between the present theory and $\rho_f^{(S)}$ so far as large ω is concerned. Near the Fermi level, on the other hand, the heights of the Kondo resonance are considerably different from each other as shown in the inset

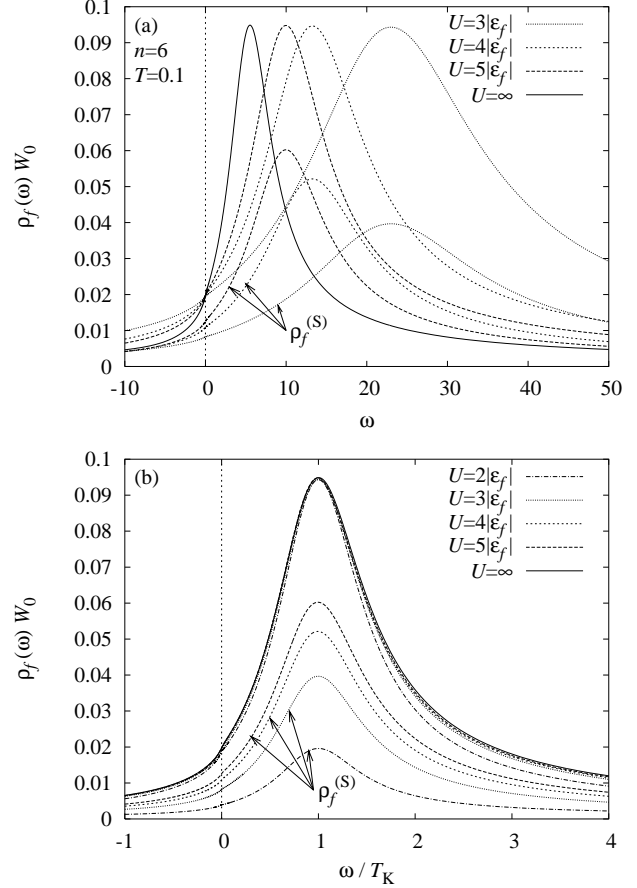


Fig. 6. Single-particle spectra near the Fermi level for several values of U with $n = 6$, $W_0 = 30$ and $\epsilon_f = -1200$ at $T = 0.1$.

of Fig. 5(a). This is mainly due to different values for the Kondo temperature T_K in different approximation schemes. At much lower temperature $T = 0.1$, we can actually see from Fig. 5(b) that the heights of the Kondo resonance peak are almost the same, except for $\rho_f^{(S)}$. It is known that the peak position with large n roughly gives T_K ,¹⁹ which also determines the zero temperature limit of the susceptibility and the Sommerfeld coefficient of the specific heat. The precise definition of T_K is discussed in the next subsection. We notice that T_K in the present theory is larger than that in the infinite- U NCA as we expect, while the energy scale becomes smaller in the $\text{NCA}f^2$. The inaccuracy of the $\text{NCA}f^2$ scheme has been pointed out in ref. 4.

In order to look through the Kondo behavior in this scheme, we show spectra near the Fermi level at low enough temperatures compared with the Kondo energy scale. Figure 6(a) shows spectra for several values of U with $n = 6$. In addition to results in the present scheme, $\rho_f^{(S)}$ is shown for comparison. Characteristic energy scales turn out to increase as U decreases. We define the Kondo temperature T_K by the peak position of the resonance, and show rescaled spectra as a function of ω/T_K in Fig. 6(b). The spectra for $U \geq 3|\epsilon_f|$ are almost identical to each other, while the spectrum for $U = 2|\epsilon_f|$ is a little different from the others. The excellent scaling property of the Kondo resonance ensures an accuracy of

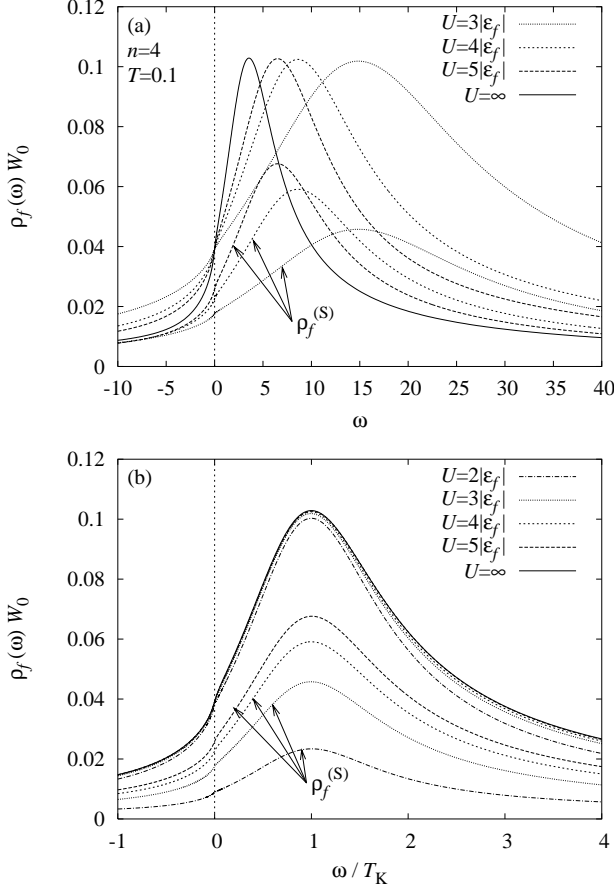


Fig. 7. Single-particle spectra near the Fermi level for several values of U with $n = 4$, $W_0 = 45$ and $\epsilon_f = -1200$ at $T = 0.1$.

the calculated intensity in the present scheme. On the other hand, $\rho_f^{(S)}$ clearly fails to demonstrate the scaling property. The vertex correction in the Green function consequently turns out essential to reproduce the universal behavior of the Kondo systems. Spectra of $n = 4$ also exhibit the scaling property as shown in Fig. 7.

Figure 8 shows W_0 dependence of spectra with $n = 6$ and $U = 6000$. The ordinate is the density of states multiplied by W_0 . The peak heights in the scaled ordinate are nearly identical, which is also consistent with the scaling property as expected.

4.2 The Kondo temperature

We employ the definition of T_K as the energy scale of the system at zero temperature.^{20,21} Namely the $4f$ magnetic susceptibility χ at $T = 0$ determines T_K by

$$\chi = Cn_f/T_K, \quad (22)$$

where C is the Curie constant. Assuming $n_f = 1$ with frozen charge fluctuation, the Fermi liquid theory gives the $4f$ contribution to the specific heat coefficient γ as

$$\gamma = \frac{\pi^2}{3T_K} \frac{n-1}{n}. \quad (23)$$

In the Fermi liquid theory, the quasi-particle density of states $\rho_f^*(0)$ per spin-orbital channel at the Fermi level determines γ as $\gamma = n\pi^2\rho_f^*(0)/3$. On the other hand, the

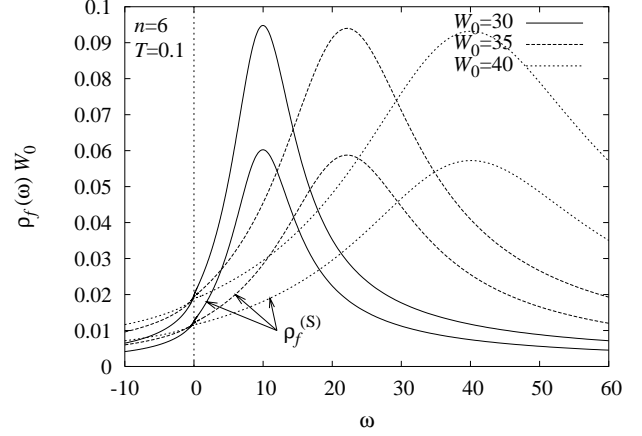


Fig. 8. Single-particle spectra near the Fermi level for several values of W_0 at $T = 0.1$ with parameters $n = 6$, $\epsilon_f = -1200$ and $U = 5|\epsilon_f| = 6000$.

original density $\rho_f(0)$ of $4f$ states is given exactly by the Friedel sum-rule as

$$\rho_f(0) = \frac{1}{\pi^2 W_0} \sin^2 \left(\frac{\pi n_f}{n} \right). \quad (24)$$

The wave function renormalization factor a_f connects these densities of states by

$$\rho_f(0) = a_f \rho_f^*(0). \quad (25)$$

At zero temperature, an approximate analytic formula for $\rho_f(\omega)$ has been proposed,¹⁹ which interpolates the Fermi liquid result and the high-energy tail of the Kondo resonance. Between the Fermi level and the peak position of the Kondo resonance, the density of states is approximately given by^{19,20}

$$\rho_f(\omega) = \frac{a_f}{\pi} \cdot \frac{\tilde{\Delta}}{(\omega - \tilde{\epsilon}_f)^2 + \tilde{\Delta}^2}, \quad (26)$$

where $\tilde{\epsilon}_f$ and $\tilde{\Delta}$ are the renormalized $4f^1$ level and its width, respectively. Requiring the same number of $4f$ electrons and $4f$ quasi-particles, we obtain the relation

$$\tilde{\Delta}^2/(\tilde{\epsilon}_f^2 + \tilde{\Delta}^2) = \sin^2(\pi n_f/n). \quad (27)$$

Hence the renormalization factor is given by $a_f = \tilde{\Delta}/(\pi W_0)$. Furthermore comparison with eq. (23) relates the peak position $\tilde{\epsilon}_f$ and T_K with $n_f = 1$ by²¹

$$\tilde{\epsilon}_f = \frac{n^2 \sin(\pi/n) \cos(\pi/n)}{\pi(n-1)} T_K. \quad (28)$$

Hence we can derive T_K from the peak position of $\rho_f(\omega)$. The proportionality factor in eq. (28) is 0.99 for $n = 6$ and 0.85 for $n = 4$.

We next compare the Kondo temperature T_K derived from $\rho_f(\omega)$ with analytic formula derived by the scaling theory. In the parameter regime such that $-\epsilon_f \gg D$ and $\epsilon_f + U \gg D$, a combination of the Schrieffer-Wolff transformation and the second-order scaling theory gives an analytic expression for the Kondo temperature of the form²¹

$$T_K^{(2)} = cDg^{1/n} \exp(-1/g),$$

Table I. The Kondo temperature for various sets of parameters. T_K is a value determined from the peak position of the Kondo resonance by eq. (28), and $T_K^{(2)}$ is that evaluated by eq. (29).

(a) present theory ($n = 6$, $W_0/ \epsilon_f = 0.025$)				
ϵ_f	$U/ \epsilon_f $	T_K	$T_K^{(2)}$	$T_K/T_K^{(2)}$
$-\infty$	2	238	292	0.81
$-\infty$	3	77	92	0.84
$-\infty$	4	45	52	0.88
$-\infty$	5	33	37	0.90
$-\infty$	∞	10	9.3	1.09
-1200	2	89	—	—
-1200	3	23	—	—
-1200	4	13	—	—
-1200	5	10	—	—
-1200	∞	5.5	—	—

(b) present theory ($n = 4$, $W_0/ \epsilon_f = 0.0375$)				
ϵ_f	$U/ \epsilon_f $	T_K	$T_K^{(2)}$	$T_K/T_K^{(2)}$
$-\infty$	2	201	264	0.76
$-\infty$	3	67	80	0.83
$-\infty$	4	40	45	0.89
$-\infty$	5	30	32	0.94
$-\infty$	∞	9.9	7.9	1.25
-1200	2	70	—	—
-1200	3	18	—	—
-1200	4	10	—	—
-1200	5	7.6	—	—
-1200	∞	4.2	—	—

(c) NCA f^2 ($n = 6$, $W_0/ \epsilon_f = 0.025$)				
ϵ_f	$U/ \epsilon_f $	T_K	$T_K^{(2)}$	$T_K/T_K^{(2)}$
$-\infty$	2	7.9	292	0.027
$-\infty$	3	9.6	92	0.15
$-\infty$	4	9.8	52	0.19
$-\infty$	5	10	37	0.27
$-\infty$	∞	10	9.3	1.09

$$g = nW_0[|\epsilon_f|^{-1} + (U + \epsilon_f)^{-1}], \quad (29)$$

where c is a numerical constant of the order of unity, which cannot be determined by the scaling theory. We fix c as unity in this paper for simplicity. If the parameters are such that $-\epsilon_f < D$ or $\epsilon_f + U < D$, conduction band states with excitation energies around D do not participate in renormalization processes for the Kondo screening. Then the cut-off energies are given roughly by $\max\{-D, \epsilon_f\}$ for the lower and $\min\{D, \epsilon_f + U\}$ for the upper. In such a case, estimate of T_K becomes more complicated.^{21,22} In order to avoid the complexity, we solve integral equations under the Coqblin-Schrieffer limit, that is, $-\epsilon_f, U, W_0 \rightarrow \infty$ with g fixed. Then eq. (29) is valid for comparison with the present theory. The limit is taken at the stage of integral equations by introducing auxiliary functions such as $\tilde{J}_0(z) = -W_0 R_0(z)$ and $\Pi_0(z) = \Sigma_0(z)/W_0$ that remain finite under the limit operation.⁸

Table I shows T_K and $T_K^{(2)}$, determined respectively by eqs. (28) and (29), for several values of parameters. Table I(a) shows that the present theory gives a reasonable agreement with $T_K^{(2)}$ in $n = 6$ over a wide range of U . Deviations from $T_K^{(2)}$ become larger in the case of small U . We attribute the deviations to the approximation for the vertex function, which neglects energy dependence of the $4f^2$ resolvent in the renormalization processes. In the

Table II. Integrated density of states of $4f$ electrons in the present scheme evaluated by eqs. (16) and (21), and the exact value by eq. (19), with $\epsilon_f = -1200$ and $T = 0.1$.

(a) $n = 6$, $W_0 = 30$		
$U/ \epsilon_f $	(present theory)	(exact)
2	1.53	0.962
3	1.13	0.975
4	1.07	0.983
5	1.05	0.988

(b) $n = 4$, $W_0 = 45$		
$U/ \epsilon_f $	(present theory)	(exact)
2	1.48	0.972
3	1.14	0.983
4	1.08	0.989
5	1.05	0.992

case of $n = 4$, on the other hand, variation of $T_K/T_K^{(2)}$ for different values of $U/|\epsilon_f|$ is larger than the case of $n = 6$. This is mainly attributed to neglect of higher order terms in the $1/n$ expansion. Namely the present theory ($U < \infty$) neglects many contributions of order $1/n$ and beyond, while the original NCA ($U = \infty$) keeps all $1/n$ order terms but neglects some $1/n^2$ contributions.

We can see from Table I(a) and (b) that the $4f^0$ and $4f^2$ levels lying within the conduction band lead to quite lower values of T_K as compared to the case of the Coqblin-Schrieffer limit. The reduction of T_K should be due to the smaller cut-off energies caused by the virtual charge excitations.

Table I(c) shows T_K evaluated with use of the NCA f^2 . No enhancement of T_K by finite values of U is obtained by this lowest order self-consistent approximation. We thus conclude that inclusion of higher order terms of the vertex correction is the essence of the present theory which gives the proper energy scale of the Kondo effect.

4.3 Sum-rules and exact relations

We now examine whether the present theory satisfies the exact sum-rules. Table II shows the integrated density of states in the present theory determined by eqs. (16) and (21), together with the exact value given by eq. (19). Note that the deviation from the exact value becomes larger as U decreases, while it is not affected by the value of n . We accordingly attribute the inaccuracy of integrated density of states to the approximation of the vertex function, because the NCA f^2 v scheme has a conserving property provided the integral equation (4) is solved exactly. We further conclude that the large intensity comes from the $4f^2$ part at high energy regime above the Fermi level. The conclusion is based on the following two reasons: first the particle number is not affected by the vertex correction, and secondly the Kondo resonance peak near the Fermi level shows the proper scaling behavior. We have confirmed that the deviation from the sum rule becomes smaller at higher temperatures.

Table III shows $\rho_f(0)$ obtained in the present scheme at $T = 0.1$ and the exact value at $T = 0$ evaluated from n_f by eq. (24). The deviations from the exact values are roughly 10 percent in $n = 6$, and 15 percent in $n = 4$. The deviations are insensitive to the parameter U . Thus

Table III. The value $\rho_f(0)W_0$ obtained in the present theory at $T = 0.1$, and the exact value at $T = 0$ evaluated from n_f by eq. (24), with parameter $\epsilon_f = -1200$.

(a) $n = 6, W_0 = 30$			
$U/ \epsilon_f $	(present theory)	(exact)	n_f
2	0.0192	0.0220	0.926
3	0.0196	0.0228	0.944
4	0.0197	0.0228	0.944
5	0.0198	0.0219	0.942
∞	0.0198	0.0219	0.925

(b) $n = 4, W_0 = 45$			
$U/ \epsilon_f $	(present theory)	(exact)	n_f
2	0.0388	0.0448	0.926
3	0.0391	0.0457	0.938
4	0.0392	0.0456	0.936
5	0.0392	0.0453	0.933
∞	0.0391	0.0441	0.917

the present theory is not worse than the original NCA in deriving $\rho_f(0)$. It is known that a fictitious anomaly appears at the Fermi level due to the inaccuracy of the NCA at $T = 0$.²³ We can recognize tiny spikes at the Fermi level in Figs. 6 and 7. Note that the anomaly in $n = 6$ is smaller than that in $n = 4$. As in the original NCA, the present theory does not give exact description of the Fermi liquid property.

4.4 Thermodynamics

We now present numerical results for thermodynamic quantities of $4f$ contribution, and then examine adequacy of the present theory for the Kondo effect. The partition function Z_f of $4f$ part is given in terms of the resolvents by eq. (3). The entropy S_f and specific heat C_f of $4f$ contribution can be computed by numerical differentiations of Z_f with respect to temperature. To obtain reasonable numerical accuracy, however, it requires computations at numerous values of temperature, especially for the second derivatives. Following ref. 24, we derive temperature derivatives of resolvents by solving additional integral equations. In this way thermodynamic quantities are computed without numerical differentiations.

Figure 9(a) shows the entropy as a function of temperature for several values of U with $n = 6$. The entropy exhibits reduction from $\ln 6$ toward lower temperature due to the Kondo screening. The characteristic energy scale becomes large with decreasing U as in the single-particle excitation spectra. At low temperatures, the entropy is slightly less than zero because of the inaccuracy of the NCA and the present theory. On the other hand, values larger than $\ln 6$ at high temperatures come from charge fluctuations involving $4f^0$ and $4f^2$ states. Figures 9(b) and (c) show temperature dependence of the specific heat C_f and C_f/T , respectively. The T -linear behavior of C_f , namely C_f/T being constant, is clearly seen at low temperatures. When temperature is scaled by T_K listed in Table I, C_f/T 's with different values of U become almost identical to each other as shown in the inset of Fig. 9(c). Equation (23) gives $\gamma T_K \simeq 2.74$ for $n = 6$, and is consistent with numerical results in the inset of Fig. 9(c). Thus the present theory with $n = 6$ demonstrates the

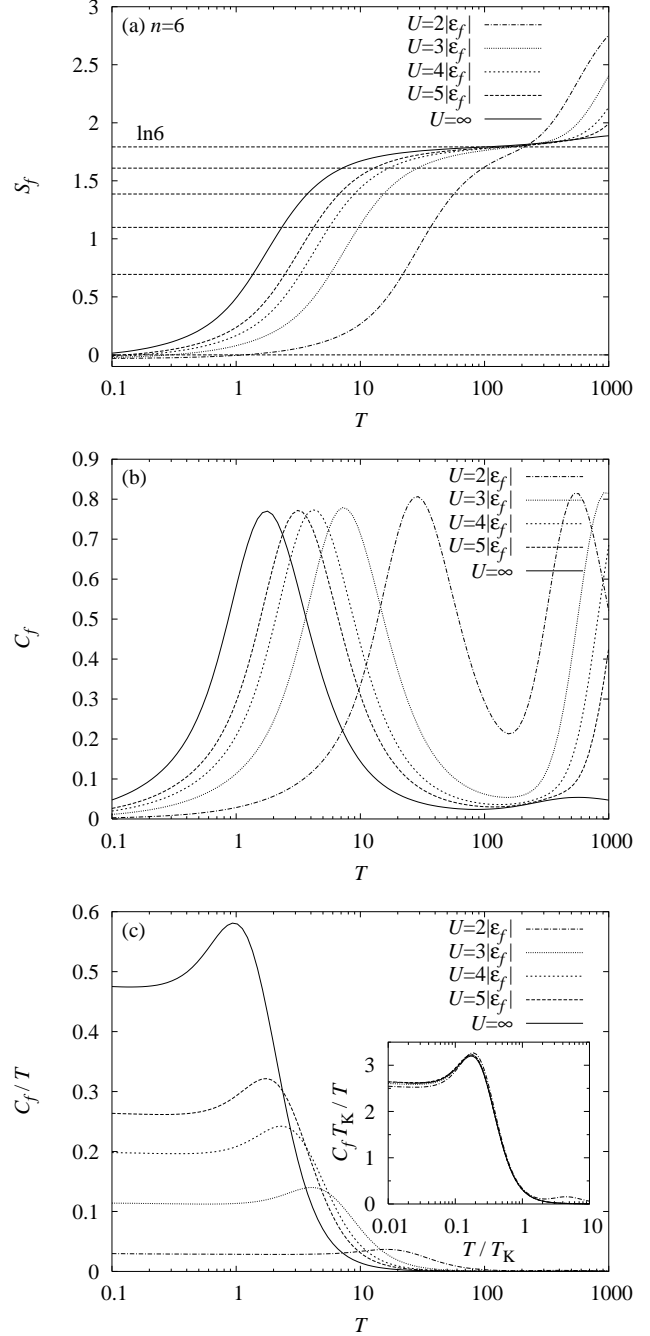


Fig. 9. Temperature dependence of the entropy S_f and the specific heat C_f of $4f$ contribution for several values of U with $n = 6$. Other parameters are same as Fig. 6. The values of T_K are listed in Table I(a).

scaling property of the Kondo effect in the specific heat as well as the single-particle spectrum.

On the other hand, thermodynamic quantities with $n = 4$ show larger inaccuracy. The minus values of the entropy at low temperatures are seen more clearly than the $n = 6$ case in Fig. 10(a). Although the scaling behavior retains as shown in the inset of Fig. 10(c), C_f/T does not stay constant with decreasing temperature. Thus in the case of $n = 4$, the present theory (and the original NCA) has a limited accuracy to describe the specific heat at low temperatures.

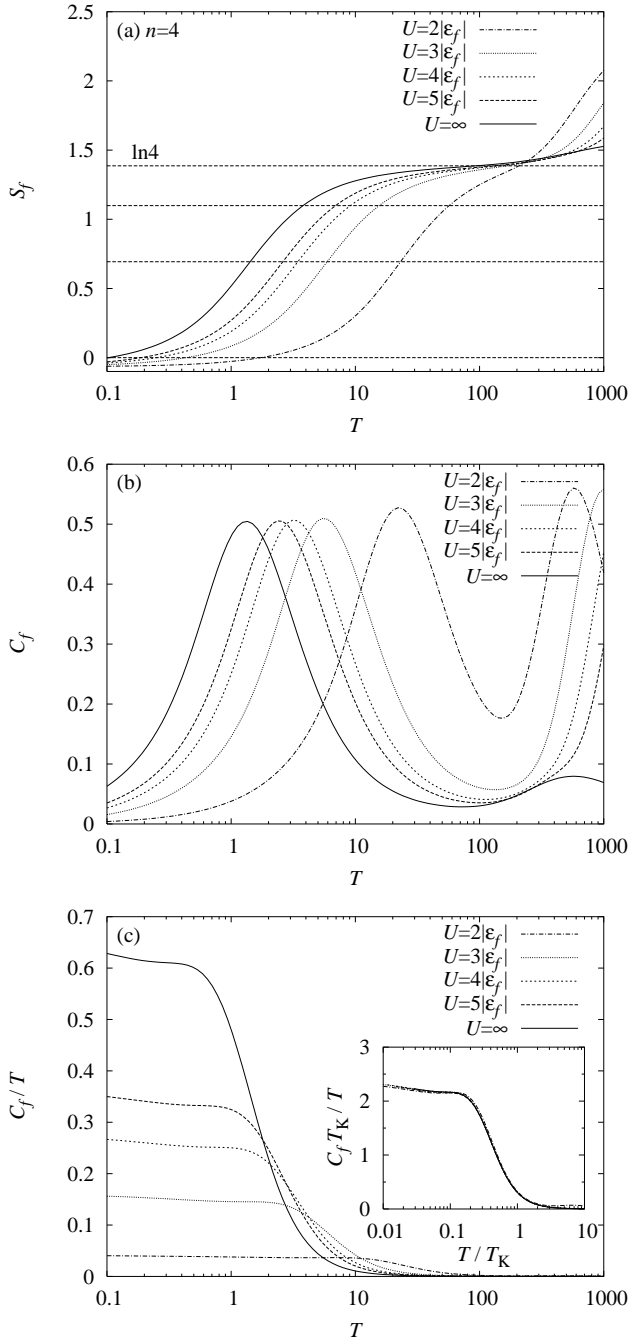


Fig. 10. Temperature dependence of the entropy S_f and the specific heat C_f of $4f$ contribution for several values of U with $n = 4$. Other parameters are same as Fig. 7. The values of T_K are listed in Table I(b).

We obtain the relation between χ and γ by combining eqs. (22) and (23) in the form independent of T_K as follows:

$$\frac{\gamma C}{\chi} = \frac{\pi^2}{3} \frac{n-1}{n}. \quad (30)$$

Derivation of the magnetic susceptibility for $U < \infty$ is much more complicated than the $U = \infty$ case because of the $4f^2$ contribution. Hence we check the accuracy in description of thermodynamics by returning to the original NCA ($U = \infty$). Figure 11 shows temperature dependence of the susceptibility computed in the NCA. From

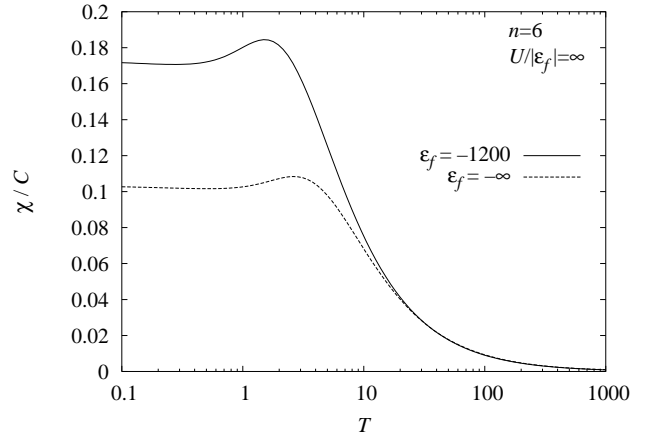


Fig. 11. Temperature dependence of the static magnetic susceptibility computed in the NCA with $n = 6$ and $W_0/|\epsilon_f| = 0.025$. C is the Curie constant.

Figs. 9 and 11 we obtain $\gamma C/\chi = 2.77$ at $T = 0.1$, while eq. (30) gives 2.74. Thus the NCA ($U = \infty$) describes with a reasonable accuracy the universal behavior in the specific heat and the static susceptibility.

5. Summary

We have derived the single-particle spectrum within the conserving scheme, following the NCA f^2v approximation. The theory incorporates infinite skeleton diagrams of leading contributions in the $1/n$ expansion. Equations have been simplified by approximations that are justifiable under the conditions of large- n and large- U . Resultant formulations have forms quite similar to those of the lowest order approximation: the equations for the Green function as well as the resolvents are obtained from the lowest order formulae by only replacing $\Sigma_0(z)$ by $\Sigma_0(z)\Lambda(z)$, and $R_0(z)$ by $R_0(z)\Lambda(z)^2$. The vertex function $\Lambda(z)$ has been given analytically.

Numerical calculations have shown that the scaling behavior of the Kondo resonance is well reproduced by the present theory. Thermodynamical quantities computed in the scheme are properly scaled by the characteristic energy as well. Furthermore, the Kondo temperature T_K has turned out to be consistent with analytic estimate for $n = 6$ over a wide range of the Coulomb repulsion U . Although the present scheme breaks the sum-rule of the spectrum due to the simplification in actual calculations, the inaccuracy in intensity comes only from the $4f^2$ peak at high energy regime. Thus the drawback does not affect the density of states in the vicinity of the Fermi level. In addition, the inaccuracy remains small as long as U is so large that the relation $|\epsilon_f| < \epsilon_f + U$ holds. This is the case in most of Ce compounds.

The present theory has the advantage that it hardly requires extra time for computations as compared to the lowest order self-consistent approximation. Consequently, the theory is easily applicable to the DMFT, and to models with complex $4f$ levels and realistic band structures.

Acknowledgment

We acknowledge useful discussion with Prof. O. Sakai, and suggestion of Dr. H. Kusunose on the Kondo temperature.

Appendix: Equations for the Defect Propagator

Single-particle excitation has been represented in terms of two types of spectral functions $\eta_\gamma(\omega)$ and $\xi_\gamma(\omega)$ defined by eqs. (14) and (15). Although $\xi_\gamma(\omega)$ is related to $\eta_\gamma(\omega)$ analytically, it is difficult to compute $\xi_\gamma(\omega)$ directly due to the Boltzmann factor. Following ref. 23, we transform original equations for the resolvent into equivalent but more convenient forms, and calculate $\xi_\gamma(\omega)$ by numerical iterations.

In order to make expressions simple, we introduce an operator \mathcal{P} defined by $\mathcal{P}R_\gamma(\omega) = -Z_f^{-1}e^{-\beta\omega}\pi^{-1}\text{Im}R_\gamma(\omega + i\delta)$. With use of the operator \mathcal{P} , we define $\sigma_\gamma(\omega) = \mathcal{P}\Sigma_\gamma(\omega)$ and $\xi_\Lambda(\omega) = \mathcal{P}\Lambda(\omega)$. Operating \mathcal{P} on eqs. (2) and (5), we obtain

$$\xi_\gamma(\omega) = |R_\gamma(\omega + i\delta)|^2 \sigma_\gamma(\omega), \quad (\text{A}\cdot 1)$$

$$\xi_\Lambda(\omega) = (n-1)\tilde{R}_2|\Lambda(\omega + i\delta)|^2\tilde{\sigma}_0^{(\text{NCA})}(\omega), \quad (\text{A}\cdot 2)$$

where $\tilde{\sigma}_0^{(\text{NCA})}(\omega)$ is defined by $\tilde{\sigma}_0^{(\text{NCA})}(\omega) = \mathcal{P}\tilde{\Sigma}_0^{(\text{NCA})}(\omega)$ and is calculated by

$$\tilde{\sigma}_0^{(\text{NCA})}(\omega) = \int d\epsilon W(\epsilon) f(-\epsilon) \xi_1(\omega + \epsilon), \quad (\text{A}\cdot 3)$$

which follows from an operation of \mathcal{P} on eq. (6). Similarly, operations of \mathcal{P} on eqs. (7), (8) and (10) yield equations for $\sigma_\gamma(\omega)$ as follows:

$$\begin{aligned} \sigma_0(\omega) &= n\xi_\Lambda(\omega)\tilde{\Sigma}_0^{(\text{NCA})}(\omega + i\delta) \\ &\quad + n\Lambda(\omega + i\delta)^*\tilde{\sigma}_0^{(\text{NCA})}(\omega), \end{aligned} \quad (\text{A}\cdot 4)$$

$$\begin{aligned} \sigma_1(\omega) &= \int d\epsilon W(\epsilon) [f(\epsilon)\tilde{\xi}_0(\omega - \epsilon) \\ &\quad + (n-1)f(-\epsilon)\xi_2(\omega + \epsilon)], \end{aligned} \quad (\text{A}\cdot 5)$$

$$\sigma_2(\omega) = 2 \int d\epsilon W(\epsilon) f(\epsilon) \xi_1(\omega - \epsilon), \quad (\text{A}\cdot 6)$$

where $\tilde{\xi}_0(\omega)$ is defined by $\tilde{\xi}_0(\omega) = \mathcal{P}\tilde{R}_0(\omega)$. Equation (9) leads to an explicit expression

$$\begin{aligned} \tilde{\xi}_0(\omega) &= \xi_0(\omega)\text{Re}[\Lambda(\omega + i\delta)^2] \\ &\quad + 2\text{Re}[R_0(\omega + i\delta)]\text{Re}[\Lambda(\omega + i\delta)]\xi_\Lambda(\omega). \end{aligned} \quad (\text{A}\cdot 7)$$

These linear equations, (A·1)–(A·7), do not determine norms of $\xi_\gamma(\omega)$, $\sigma_\gamma(\omega)$. The norms can be determined by the following sum-rule:

$$\int d\omega \sum_\gamma \xi_\gamma(\omega) = 1. \quad (\text{A}\cdot 8)$$

This identity follows from eq. (3). Normalizing by eq. (A·8) is equivalent to determination of the partition function, and thus thermodynamics is obtained by a combination of $\eta_\gamma(\omega)$ and $\xi_\gamma(\omega)$.²⁴

- 1) A. Georges, G. Kotliar, W. Krauth and M. J. Rozenberg: *Rev. Mod. Phys.* **68** (1996) 13.
- 2) I. A. Nekrasov, . Held, N. Blümer, A. I. Poteryaev, V. I. Anisimov and D. Vollhardt: *Eur. Phys. J. B* **18** (2000) 55.
- 3) M. B. Zöhl, I. A. Nekrasov, Th. Pruschke, V. I. Anisimov and J. Keller: *Phys. Rev. Lett.* **87** (2001) 276403.
- 4) O. Sakai, Y. Shimizu and Y. Kaneta: *J. Phys. Soc. Jpn.* **74** (2005) 2517.
- 5) Y. Kuramoto: *Z. Phys. B* **53** (1983) 37; H. Kojima, Y. Kuramoto and M. Tachiki: *Z. Phys. B* **53** (1984) 293.
- 6) N. Grewe: *Z. Phys. B* **53** (1983) 271.
- 7) H. Keiter and G. Morandi: *Phys. Rep.* **109** (1984) 227.
- 8) N. E. Bickers: *Rev. Mod. Phys.* **59** (1987) 845.
- 9) P. Coleman: *Phys. Rev. B* **29** (1984) 29.
- 10) K. G. Wilson: *Rev. Mod. Phys.* **47** (1975) 773.
- 11) J. E. Hirsch and R. M. Fye: *Phys. Rev. Lett.* **56** (1986) 2521.
- 12) Y. Kuramoto: in *Theory of Heavy Fermions and Valence Fluctuations*, ed. T. Kasuya and T. Saso (Springer-Verlag, Berlin, 1985) p. 152.
- 13) C.-I. Kim, Y. Kuramoto and T. Kasuya: *J. Phys. Soc. Jpn.* **59** (1990) 2414.
- 14) Th. Pruschke, D. L. Cox and M. Jarrell: *Phys. Rev. B* **47** (1993) 3553.
- 15) O. Sakai, M. Motizuki and T. Kasuya: in *Core-Level Spectroscopy in Condensed Systems Theory*, ed. J. Kanamori and A. Kotani (Springer-Verlag, Berlin, 1988) p. 45.
- 16) Th. Pruschke and N. Grewe: *Z. Phys. B* **74** (1989) 439.
- 17) T. Saso: *Prog. Theor. Phys. Suppl.* **108** (1992) 89.
- 18) K. Haule, S. Kirchner, J. Kroha and P. Wölfle: *Phys. Rev. B* **64** (2001) 155111; J. Kroha and P. Wölfle: *J. Phys. Soc. Jpn.* **74** (2005) 16.
- 19) Y. Kuramoto and E. Müller-Hartmann: *J. Magn. Magn. Mater.* **52** (1985) 122.
- 20) Y. Kuramoto and Y. Kitaoka: *Dynamics of Heavy Electrons* (Oxford University Press, 2000).
- 21) A. C. Hewson: *The Kondo Problem to Heavy Fermions* (Cambridge University Press, 1993).
- 22) F. D. M. Haldane: *J. Phys. C* **11** (1978) 5015.
- 23) Y. Kuramoto and H. Kojima: *Z. Phys. B* **57** (1984) 95.
- 24) J. Otsuki, H. Kusunose and Y. Kuramoto: *cond-mat/0510424*.